# Transition State Analysis for Human and *Plasmodium falciparum* Purine Nucleoside Phosphorylases†

Andrzej Lewandowicz and Vern L. Schramm*

*Department of Biochemistry, Albert Einstein College of Medicine, 1300 Morris Park Avenue, Bronx, New York 10461*

*Received October 27, 2003*

ABSTRACT: Recent studies have shown that *Plasmodium falciparum* is sensitive to a purine salvage block at purine nucleoside phosphorylase (PNP) and that human PNP is a target for T-cell proliferative diseases. Specific tight-binding inhibitiors might be designed on the basis of specific PNP transition state structures. Kinetic isotope effects (KIEs) were measured for arsenolysis of inosine catalyzed by *P. falciparum* and human purine nucleoside phosphorylases. Intrinsic KIEs from [1′-$^3$H]-, [2′-$^3$H]-, [1′-$^{14}$C]-, [9-$^{15}$N]-, and [5′-$^3$H]inosines were 1.184 ± 0.004, 1.031 ± 0.004, 1.002 ± 0.006, 1.029 ± 0.006, and 1.062 ± 0.002 for the human enzyme and 1.116 ± 0.007, 1.036 ± 0.003, 0.996 ± 0.006, 1.019 ± 0.005, and 1.064 ± 0.003 for *P. falciparum* PNPs, respectively. Analysis of KIEs indicated a highly dissociative $D_N$*$A_N$ ($S_N$1) stepwise mechanism with very little leaving group involvement. The near-unity 1′-$^{14}$C KIEs for both human and *P. falciparum* PNP agree with the theoretical value for a 1′-$^{14}$C equilibrium isotope effect for oxacarbenium ion formation when computed at the B1LYP/6-31G(d) level of theory. The 9-$^{15}$N KIE for human PNP is also in agreement with theory for equilibrium formation of hypoxanthine and oxacarbenium ion at this level of theory. The 9-$^{15}$N KIE for *P. falciparum* PNP shows a constrained vibrational environment around N9 at the transition state. A relatively small $\beta$-secondary 2′-$^3$H KIE for both enzymes indicates a 3′-*endo* conformation for ribose and relatively weak hyperconjugation at the transition state. The large 5′-$^3$H KIE reveals substantial distortion at the 5′-hydroxymethyl group which causes loosening of the C5′−H5′ bonds during the reaction coordinate.

*Plasmodium falciparum* (*P.f.*)[1] is the main cause of life-threatening malaria. It is increasingly difficult to control due to multidrug resistance (*1*, *2*). The finding of alternative antimalarial targets is crucial for the development of other therapeutic approaches. It has long been proposed that the purine salvage pathway may be an antimalarial target (*3*, *4*). *P. falciparum* is unable to synthesize purines and requires purines supplied from its host for DNA and RNA synthesis. Hypoxanthine has been identified as the most common precursor of purine nucleosides in *P. falciparum*, and its requirement causes *P.f.* to be sensitive to PNP inhibition. PNP inhibition causes purine-less death of the parasite (*5*−*7*). Transition state analogues exhibit high specificity for enzymatic transition states, and it may be possible to develop inhibitors specific for human and malarial isozymes. It is still unknown if inhibition of both human and *P.f.* PNP is required to inhibit growth of *P.f.* Details of both the human and *P.f.* transition states are required for the initiation of isozyme specific inhibitor design. At present, only the structure of the bovine PNP transition state is known.

Human PNP is an important target for T-cell-related cancers and autoimmune diseases (*8*−*11*). Dividing T-cells express deoxycytidine kinase which salvages deoxycytidine to dCMP for DNA synthesis (*12*). The high level of dGuo that accumulates under impaired PNP activity is a substrate for deoxycytidine kinase which converts it to dGMP. Accumulation of dGTP allosterically blocks ribonucleotide diphosphate reductase, and the resulting deoxynucleotide depletion causes apoptotic cell death (*13*, *14*). Immucillin-H is a PNP transition state analogue that inhibits the division of T-cells without affecting noninduced T-lymphocytes or any other dividing cells (*8*). Under normal conditions, the blood level of deoxyguanosine is less than 10 nM because of high levels of PNP in human tissues, but in PNP-deficient patients, the deoxyguanosine level in blood can reach 10 $\mu$M, causing it to accumulate as dGTP in stimulated T-cells (*15*).

Transition state theory predicts that enzymes stabilize the transition state structure rather than substrate, binding to it with high affinity. Although transition state structure is nebulous, kinetic isotope effects are a potent tool for its analysis (*16*−*19*). Kinetic isotope effects (KIEs) define the ratio of reaction rates for the normal and labeled reactant ($k_{light}/k_{heavy}$). KIEs reflect changes in the vibrational environment from free reactants to the transition state, where the transition state is the highest energetic barrier in the reaction coordinate. If the labeled atom is more constrained in the ground state than in the transition state, kinetic isotope effects are normal and the light molecule reacts faster. The heavy isotopomer reacts more rapidly when the heavy atom is more vibrationally constrained at the transition state. In general, KIEs reflect alteration in bond strength at an atomic center on conversion from the free molecule to the transition

† This work was supported by National Institutes of Health Grants AI49512 and GM41916.

* To whom correspondence should be addressed. Telephone: (718) 430-2813. Fax: (718) 430-8565. E-mail: vern@aecom.yu.edu.

[1] Abbreviations: PNP, purine nucleoside phosphorylase; *P.f.*, *P. falciparum*; dGuo, 2′-deoxyguanosine; KIE, kinetic isotope effect; EIE, equilibrium isotope effect; LB, Luria broth; DFT, density functional theory; LYP, correlation functional of Lee, Yang, and Parr; DADMe-ImmH, 4′-deaza-1′-aza-2′-deoxy-1′-(9-methylene)-Immucillin-H; ImmH, Immucillin-H; MEP, molecular electrostatic potential.

10.1021/bi0359123 CCC: $27.50 
Published on Web 01/22/2004

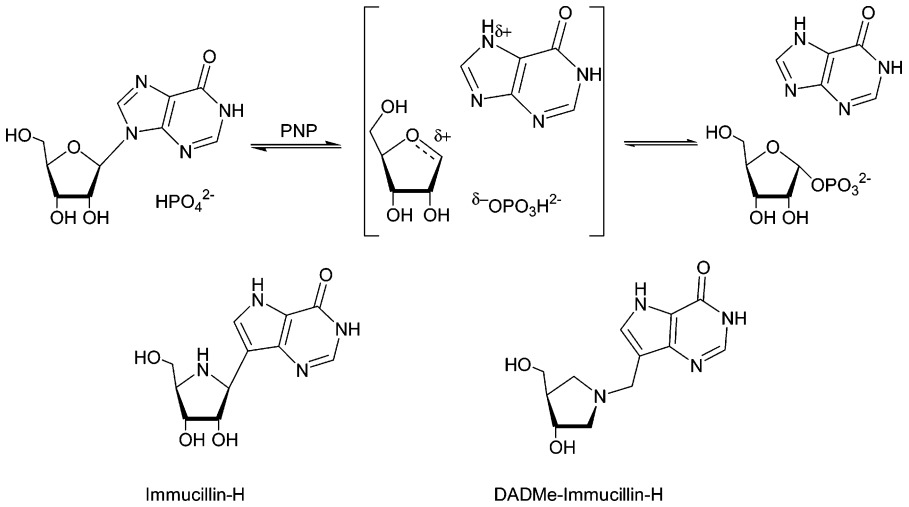


FIGURE 1: Inosine phosphorolysis catalyzed by purine nucleoside phosphorylase. The hypoxanthine leaving group and phosphate nucleophile are well-separated from the ribooxacarbenium ion. Two transition state analogue inhibitors are shown in their neutral forms, but are partially cationic at neutral pH values (*16*).

state (*20*). Equilibrium isotope effects (EIEs) reflect bond vibrational differences between stable reactant states.

Competitive KIE measurements provide $V_{max}/K_m$ isotope effects up to and including the first irreversible step. Irreversible steps prior to the transition state prevent a KIE and must be identified and corrected to provide intrinsic effects for transition state analysis.

KIE analysis for bovine PNP was reported earlier and indicated that the enzyme catalyzes inosine phosphorolysis according to a dissociative $S_N2$ mechanism ($D_NA_N$; see ref *39* for terminology). At the transition state, the bond order is 0.38 in the C1′−N9 bond but the bond order for the bond to $PO_4$ is very weak (*21*). Immucillin-H was designed as a transition state analogue of bovine PNP and has an equilibrium dissociation constant $K_i$* of 23 pM, and the $K_i$* was 56 pM for human PNP (*22*). Recently, DADMe-ImmH was shown to have even tighter binding ($K_i$* = 16 pM) for human PNP (*23*, *24*). This compound was designed to mimic the product side of an early transition state or a fully dissociated transition state. DADMe-ImmH has a C1′−N9 linear distance of 2.5 Å, versus 1.5 Å in Immucillin-H (Figure 1).

In contrast to the concerted bimolecular $D_NA_N$ ($S_N2$) mechanism of bovine PNP, the ricin A chain catalyzes a specific adenine depurination in RNA through a stepwise $D_N$*$A_N$ ($S_N1$) mechanism with an oxacarbenium intermediate (*25*). An irreversible, isotopically insensitive second step was consistent with expression of equilibrium isotope effects, indicating a relatively stable oxacarbenium ion intermediate.

Kinetic isotope effect analysis of human and *P. falciparum* purine nucleoside phosphorylases catalyzing inosine arsenolysis is reported here. Comparison with the transition state structures for bovine PNP and other purine nucleoside *N*-ribosyl transferases indicates substantial differences. These differences are important for future transition state analogue design with discrimination of the malarial PNP isozyme.

## MATERIALS AND METHODS

*Human Purine Nucleoside Phosphorylase (hPNP) Preparation.* Polymerase chain reaction (PCR) was used to amplify the PNP reading frame from pEPD containing human PNP (provided by S. McIvor, Institute of Human Genetics; *26*). Primers were purchased from Invitrogen. The forward primer (5′-ATGGAGAACGGATACACCTATG-3′) and reverse primer with attached stop codon (5′-TCAACTGGCTTTGTCAGGGAG-3′) flanked the ends of the open reading frame. After 35 cycles of PCR with Taq DNA polymerase (Invitrogen Corp., Carlsbad, CA; denaturation for 0.5 min at 94 °C, annealing for 1 min at 55 °C, and extension for 1.5 min at 72 °C), the reaction mixture was incubated for 30 min at 72 °C for polyadenylation. The product was a single band corresponding to approximately 1 kb as determined by agarose gel electrophoresis. The PCR product was cloned into pCR T7/NT-TOPO (Invitrogen) with an N-terminal His tag sequence and transformed into TOP10F′ "one shot" *Escherichia coli* cells (Invitrogen). Cells were plated on LB agar with 100 $\mu$g/mL ampicillin and grown overnight. Ten colonies were subcultured, and the plasmids were purified using a QIAprep Spin Miniprep Kit according to the QIAprep Miniprep Handbook. Restriction analysis with *Bam*HI and *Eco*RI (New England Biolabs) identified positive clones. Agarose gel electrophoresis visualized a band around 1 kb corresponding to human PNP with additional up- and downstream sequences. The sequence was verified by automated DNA sequencing.

*Transformation and Expression. E. coli* BL21(DE3) cells were transformed with the pCRT7/NT-TOPO-PNP plasmid (Invitrogen) and grown in medium with ampicillin (100 $\mu$g/mL) at 37 °C to achieve an optical density $OD_{600}$ of 0.3. The bacterial pellet (10 min at 4000 rpm) was resuspended in 5 mL of fresh LB with ampicillin, added to 1 L of fresh LB medium with ampicillin, and grown to an $OD_{600}$ of 0.6 (3 h). Expression was induced with lactose (0.1%) for 9.5 h at 37 °C. Cells were harvested and frozen at −70 °C for subsequent purification.

*Purification and Protein Concentration Assays.* Cells were resuspended in 20 mL of 10 mM imidazole, 300 mM NaCl, 50 mM $KPO_4$ buffer (pH 8.0), lysozyme (0.2 mg/mL), and Proteinase Inhibitor Cocktail ($^1/_{10}$ of vial content, Sigma). After 30 min on ice, cells were disrupted with a French press (three times). After centrifugation (12 000 rpm for 20 min), the supernatant was applied to a 7 mL column of Ni−NTA resin (QIAgen, Valencia, CA). Buffer (40 mL) containing 10 mM imidazole, 300 mM NaCl, and 50 mM $Na_2HPO_4$

(pH 8.0) was applied followed by 40 mL of 20 mM imidazole, 300 mM NaCl, and 50 mM $Na_2HPO_4$ buffer (pH 8.0). Human PNP was eluted with 45 mL of 250 mM imidazole, 300 mM NaCl, and 50 mM $Na_2HPO_4$ buffer (pH 8.0). The PNP concentration was measured at 280 nm [extinction coefficient of 29.8 $mM^{-1}$, based on tryptophan ($n_{Trp}$) and tyrosine ($n_{Tyr}$) content (ExPaSy ProtParam Tool, us.expasy.org)]. The PNP solution was dialyzed to 0.1 M Tris-HCl (pH 7.5), 0.1 mM EDTA, and 0.1 mM DTT and concentrated to 16 mg/mL with a Millipore centrifugal device with 10 000 Da retention.

*Enzymes and Reagents for ATP Synthesis.* Phosphoriboisomerase (PRI), pyruvate kinase from rabbit muscle (PK), L-glutamic dehydrogenase from bovine (GDH), glucose-6-phosphate dehydrogenase from *Leuconostoc mesenteroides* (G6PDH), phosphogluconic dehydrogenase from *Torula* yeast (GPDH), myokinase from chicken muscle (MK), and hexokinase from *Saccharomyces* (HK) were purchased from Sigma. Adenine phosphoribosyltransferase (APRTase) was a generous gift from C. Grubmeyer (Temple University, Philadelphia, PA), and 5′-phosphoribosylpyrophosphate synthetase (PRPPase) was a generous gift from P. Berti (McMaster University, Hamilton, ON). Alkaline phosphatase from calf intestine and adenosine deaminase were purchased from Sigma. ATP, monopotassium α-ketoglutarate, glucose, β-nicotinamide adenine dinucleotide phosphate sodium salt ($NADP^+$), phosphoenolpyruvic acid cyclohexylammonium salt (PEP), glycylglycine, potassium chloride, mono- and dipotassium phosphates, magnesium chloride, ammonium chloride, and DL-dithiothreitol (DTT) were purchased from Sigma.

*Labeled Starting Compounds.* [1′-$^3$H]ATP, [1′-$^{14}$C]ATP, [5′-$^{14}$C]ATP, [5′-$^3$H]ATP, and [4′-$^3$H]ATP were synthesized from [2′-$^3$H]glucose, [2′-$^{14}$C]glucose, [6′-$^{14}$C]glucose, [6′-$^3$H]glucose, and [5′-$^3$H]glucose, respectively (American Amersham). [2′-$^3$H]ATP was made from [2′-$^3$H]ribose 5′-phosphate as described previously (*27*). [9-$^{15}$N]ATP was synthesized from [8-$^{13}$C/1,6,9-$^{15}$N]adenine containing 98% 9-$^{15}$N-labeled, 92% $^{13}$C-labeled, 78% 6-amino-$^{15}$N-labeled, and 22% 1-$^{15}$N-labeled derivatives (Cambridge Isotope Laboratories, Inc.). The 8-$^{13}$C kinetic isotope effect and 1-$^{15}$N KIE are assumed to be negligible.

*Labeled ATP Synthesis Procedure.* Labeled ATPs were synthesized as described previously (*21*, *28*). The reaction mixture contained 0.5 mM ATP, 5−10 μCi of labeled D-glucose, 190 mM PEP, 95 μM $NADP^+$, 20 mM α-ketoglutarate, 2.5 mM DTT, 2 mM D-glucose, 5.5 mM $NH_4Cl$, 50 mM $MgCl_2$, 50 mM KCl, 50 mM glycylglycine (pH 7.5), 2.8 mM adenine, and 135 mM potassium phosphate buffer [by adding 140 μL of 1 M potassium phosphate buffer (pH 10.75)] in a final volume of 1 mL. The final pH of the mixture was 7.4. Phosphoriboisomerase (20 units), 4 units of pyruvate kinase, 0.5 unit of L-glutamic dehydrogenase, 0.5 unit of glucose-6-phosphate dehydrogenase, 1.2 units of phosphogluconic acid dehydrogenase, 3.5 units of myokinase, and 5 units of APRTase and PRPPase were added to the mixture. The reaction was initiated by adding 0.2 unit of hexokinase and the mixture incubated at 37 °C for 7 h. Enzymes provided as ammonium sulfate suspensions were pelleted and enzyme pellets resuspended in 50 mM Tris-HCl (pH 7.5) to avoid excess ammonium sulfate. In the case of [9-$^{15}$N]ATP synthesis, labeled adenine was added as the solid powder. Alternatively, [2′-$^3$H]ATP was synthesized from [2′-$^3$H]ribose 5-phosphate and with the carrier ribose 5-phosphate at a concentration of ∼2 mM. Labeled ATP was purified by reversed phase HPLC with an Xterra Prep MS $C_{18}$ 10 μm, 7.8 mm × 150 mm column. ATP was eluted with 50 mM ammonium formate (pH 3.5) with a retention time of 7.9 min (adenine was at 16 min). After being freeze-dried, it was dissolved in 0.5 mL of water and stored at −80 °C.

*Conversion of ATP to Inosine.* ATP was converted to AMP in reaction mixtures containing 12 mM glucose, 50 mM potassium phosphate, 50 mM Tris-HCl (pH 7.8), 6 mM DTT, 52 units/mL myokinase, and 12 units/mL hexokinase for 4 h at 37 °C. Conversion of ATP to AMP was monitored by HPLC. The AMP was then converted to adenosine in the same reaction mixture by increasing the pH to 11 with alkaline phosphatase 10× buffer (Promega). The reaction was started by adding alkaline phosphatase to a concentration of ∼2 units/mL and incubated at 37 °C for 1 h. Adenosine was converted to inosine by 2 units/mL bovine adenosine deaminase for 30 min after the pH was adjusted to pH 8.0 with 1 M hydrochloric acid. Inosine was purified by HPLC with an Xterra $C_{18}$ column and eluted with ammonium acetate (pH 5.5) with 7.4% (v/v) methanol at a retention time of 14.8 min. The adenosine retention time was 34 min.

*Kinetic Isotope Effect Measurements.* Inosine arsenolysis was carried out in 50 mM disodium arsenate, 50 mM Tris-HCl (pH 7.5), and 250 μM inosine. Two parallel reactions were performed under identical conditions except for human or *P. falciparum* PNPs. The reaction progress was followed spectrophotometrically at 293 nm in a control reaction monitored by xanthine oxidase (60 milliunits/mL) coupling (*23*, *29*). Kinetic isotope effect measurements were based on the $^3$H/$^{14}$C ratio of ribose products. Partial conversion used up to 30% of the initial inosine concentration, and total conversion was achieved with excess enzyme in 8 h reactions. The initial $^3$H/$^{14}$C ratio was optimized to be 4/1.

The reaction mixtures were mixed with 100 mg of charcoal equilibrated with 100 mM D-ribose, applied to spin columns (DNA purification kit from Qiagen), and centrifuged. The effluent was collected into scintillation vials. Columns were eluted five times with 0.5 mL of 100 mM D-ribose containing 10% (v/v) ethanol. Control experiments with labeled inosine demonstrated that inosine is retained while ribose is released. After being freeze-dried, the eluate was dissolved in 1 mL of water and 12 mL of xylene-based scintillation fluid (LiquiScint, National Diagnostic). In control experiments with mixtures of known $^{14}$C- and $^3$H-labeled ribose, this procedure does not affect the isotope ratio.

The kinetic isotope effect was corrected to the 0% reaction condition using eq 1:

$$\mathrm{KIE} = \ln(1 - f)/\ln(1 - fR_f/R_\infty) \quad (1)$$

where $f$ is a fraction of product formation and $R_f$ and $R_\infty$ are the ratios of heavy to light isotopes for partial and total conversion, respectively.

Tritium and $^{14}$C counts were computed by dual-channel counting. Channel 1 was $^3$H and $^{14}$C, while channel 2 was only $^{14}$C. The total $^3$H was calculated by eq 2.

$$^3\mathrm{H(total)} = {}^3\mathrm{H(channel\ 1)} - {}^{14}\mathrm{C(channel\ 2)}r(^{14}\mathrm{C}) \quad (2)$$

where $r(^{14}C)$ is the fraction of $^{14}C$ counts in channel 1. The total $^{14}C$ counts was calculated from eq 3.

$$^{14}C(\text{total}) = {}^{14}C(\text{channel 2}) + {}^{14}C(\text{channel 2})r(^{14}C) \quad (3)$$

*Commitment Analysis.* The reverse commitment (ribose 1-arsenate return to inosine) was assumed to be zero due to the chemical irreversibility of the arsenolysis reaction. Forward commitment was determined in trapping experiments from the fraction of bound inosine converted to product during the first several catalytic turnovers in excess unlabeled inosine and arsenate (*17*, *30*). The 20 $\mu$L reaction mixtures of 30 $\mu$M human or *P.f.* PNP with 430 $\mu$M [8-$^{14}$C]inosine and 50 mM Tris-HCl (pH 7.5) were incubated for 10 s and diluted to 1 mL with 4.3 mM inosine and arsenate from 0.1 to 50 mM. After 10 s, the reaction was quenched with 100 $\mu$L of 1 M hydrochloric acid and the mixture frozen. After being concentrated to 200 $\mu$L by a freeze-drying procedure, samples were applied to an HPLC $C_{18}$ reversed phase column [ammonium acetate (pH 5.5) with 7.4% (v/v) methanol]. Hypoxanthine and unreacted inosine were collected, made to 2.5 mL; 6 mL of scintillation fluid was added, and the radioactivity was counted. The forward commitment ($C_f$) is the $k_{cat}/k_{off}$ ratio of kinetic constants, where $k_{cat}$ is the fraction of the Michaelis complex converted to product and $k_{off}$ is the fraction of inosine in the Michaelis complex escaping prior to catalysis. It was computed as the ratio of hypoxanthine to inosine radioactivity at saturating 50 mM arsenate. Controls measured the amount of hypoxanthine formed under the same conditions, but without enzyme and in the presence of enzyme without arsenate.

The intrinsic kinetic isotope effect ($KIE_{intrinsic}$) corrected for commitment was calculated from Northrop's equation (*39*) (eq 4):

$$KIE_{experiment} = \frac{KIE_{intrinsic} + C_f}{1 + C_f} \quad (4)$$

where $KIE_{experiment}$ is the experimental kinetic isotope effect and $C_f$ denotes forward commitment.

*Calculations.* Optimization of reactants, transition state models, and oxacarbenium intermediate models was performed with *Gaussian 98* (*31*) using density functional theory (DFT) with the Berny algorithm, and bond frequencies were computed for optimized structures. The one-parameter Becke (B1) exchange functional with the LYP correlation functional at standard 6-31G(d) and STO-3G basis sets were used. The B1LYP method has been parametrized to yield good quality vibrational frequencies (*32*). Kinetic isotope effects were calculated from the computed frequencies with *Isoeff 98* (*33*) on the basis of eq 5 (*34*):

$$\frac{k_L}{k_H} = \frac{\nu_L^{\neq}}{\nu_H^{\neq}} \times \prod_i^{3n-6} \frac{u_{iL}^R \sinh(u_{iH}^R/2)}{u_{iH}^R \sinh(u_{iL}^R/2)} \times \prod_i^{3n^{\neq}-7} \frac{u_{iH}^{\neq} \sinh(u_{iL}^{\neq}/2)}{u_{iL}^{\neq} \sinh(u_{iH}^{\neq}/2)} \quad (5)$$

where $k_L/k_H$ is the kinetic isotope effect, $n$ is the number of atoms, $u = h\nu/k_BT$ (where $h$ and $k_B$ are the Planck and Boltzmann constants, respectively), $T$ is the absolute temperature, and $\upsilon_i$ is the frequency of normal mode vibration. The superscript $\neq$ indicates the properties of the transition state. The isotope effects were calculated at 298 K.

Similarly, equilibrium isotope effects were computed on the basis of the equation

$$\frac{k_L}{k_H} = \frac{\nu_L}{\nu_H} \times \prod_i^{3n-6} \frac{u_{iL}^R \sinh(u_{iH}^R/2)}{u_{iH}^R \sinh(u_{iL}^R/2)} \times \prod_i^{3n-6} \frac{u_{iH}^P \sinh(u_{iL}^P/2)}{u_{iL}^P \sinh(u_{iH}^P/2)} \quad (6)$$

with modification where imaginary frequencies of the transition state ($\nu_L^{\neq}/\nu_H^{\neq}$) were omitted and the second term concerned product frequencies.

Molecular electrostatic potential surfaces were calculated by the CUBE subprogram of *Gaussian 98* and were visualized with the Molekel 4.0 package (*35*) at a density of 0.008 electron/bohr, below the van der Waals radius of 0.002 electron/bohr for better resolution (*36*).

## RESULTS AND DISCUSSION

*Intrinsic KIE* and *Commitment Correction*. The observed KIEs in competitive experiments give apparent $V_{max}/K_m$ isotope effects, including commitment factors (*37*). Intrinsic isotope effects reflect vibrational changes caused by bond breaking or formation at the transition state. In nucleophilic substitutions, the isotopically sensitive step is bond displacement but also includes binding isotope effects for the substrate (*38*). Commitment factors affect the intrinsic KIE from all atoms to the same degree. The irreversibility of arsenolysis eliminates reverse commitment. However, forward commitment resulting from conversion of the substrate of the Michaelis complex to products without equilibration with free substrate cannot be neglected. The forward commitment for arsenolysis of inosine by bovine PNP was 0.19 (*21*). If the commitment is large ($C_f \gg 0$), e.g., when $k_{forward} \gg k_{off}$ (where $k_{forward}$ denotes the conversion of the ES complex to product and $k_{off}$ to the substrate), both labeled and unlabeled substrate molecules are converted to the product with the same probability and no isotope effects are observed. Forward commitments for inosine arsenolysis catalyzed by human PNP and *P.f.* PNP at 50 mM arsenate were 0.147 and 0.105, respectively, similar to that for bovine PNP (Figure 3).

*Correction of Remote Label KIEs.* Remote carbon label 5′-$^{14}$C KIE are expected to be insignificant on the basis of the four-bond distance to the chemical site; however, remote 5′-$^{3}$H and 4′-$^{3}$H substrates demonstrate a significant KIE for bovine PNP and other *N*-ribosyltransferases and cannot be neglected (*17*). KIEs from [4′-$^{3}$H]inosine were $1.024 \pm 0.003$ and $1.009 \pm 0.002$ for human and *P.f.* PNPs, respectively. When [4′-$^{3}$H]inosine was used as the remote label, the KIEs were corrected for this remote label KIE.

*Comparison of KIEs for Human, P.f., and Bovine PNPs.* Despite the level of amino acid identity between bovine and human enzymes (86%), their transition states differ on the basis of substantial differences in intrinsic KIEs (Tables 1 and 3). *P. falciparum* PNP also passes through a transition state different from that of bovine PNP but is similar to human PNP (Tables 1−3).

*1′-$^{14}$C Isotope Effects*. A highly informative KIE for transition state determination in nucleophilic substitution is the primary $^{14}C$ KIE. These are expected to be unity for fully dissociated $S_N1$ transition states, to be in the range of 1.02−1.04 for borderline $S_N1$ reactions or highly expanded $S_N2$

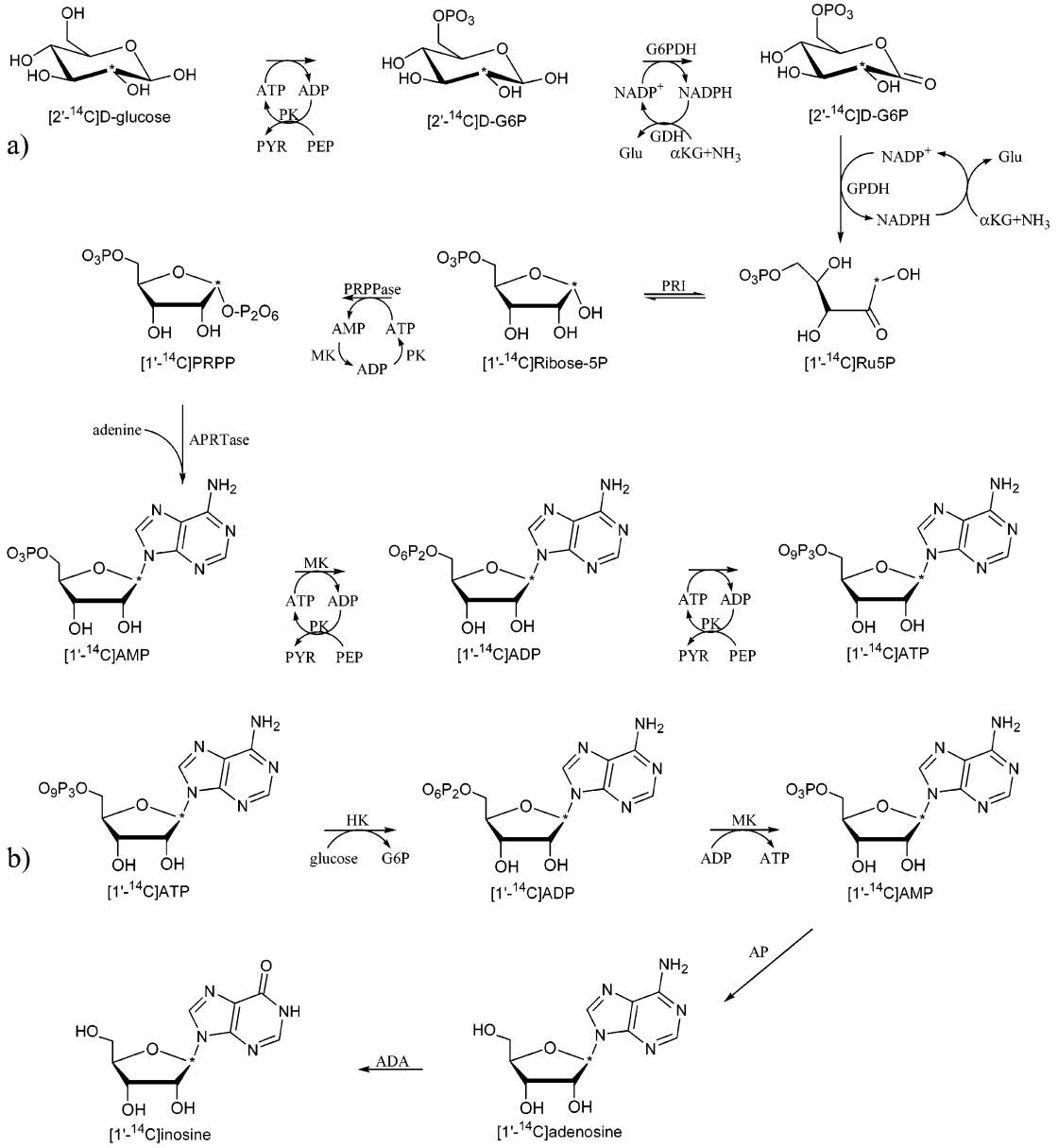


FIGURE 2: Synthesis of [1′-$^{14}$C]ATP (a) and inosine (b). See Materials and Methods for details. This example indicates the position of the $^{14}$C label with an asterisk.

mechanisms, and to approach a maximum of 1.13 for symmetric concerted nucleophilic transition states (*39*). The measured 1′-$^{14}$C kinetic isotope effects for human and *P.f.* PNPs are unity and are consistent with only a 1′-$^{14}$C equilibrium isotope effect for formation of an isolated carbocation without significant bonding to leaving or attacking groups. The 1′-$^{14}$C KIE is unity only when the contribution from reaction coordinate motion does not contribute to the KIE. Vibrational changes reflecting an altered zero-point energy (ZPE) and energy of vibrational excited states (EXC) are small for carbon atoms. Even small amounts of reaction coordinate bond order to C1′ at the transition state can be eliminated; for example, the 1′-$^{14}$C kinetic isotope effect computed at the B1LYP/6-31G(d) level of theory with a residual N9−C1′ bond order of 0.095 and a nucleophile O−C1′ bond order of 0.04 gives a large 1′-$^{14}$C KIE value of 1.11 or 1.10 for N7 unprotonated or protonated, respectively, at the transition state. The measured 1′-$^{14}$C KIE of unity matched a calculated equilibrium isotope effect (EIE) of 1.0024 between free inosine and 3′-*endo* oxacarbenium ion [B1LYP/6-31G(d) level of theory] in a dissociative $D_N$*$A_N$ ($S_N1$) mechanism where the oxacarbenium ion has a lifetime that is adequate to permit bond vibrational modes to equilibrate (Figure 4). Properties of a transition state with a fully developed oxacarbenium ion can be described on the basis of the 1′-$^{14}$C isotope effect. Any interaction of C1′ with leaving and/or attacking groups introduces some measure of the reaction coordinate motion to the isotope effect, and this invariably gives a KIE of greater than unity. Therefore, the transition state must have properties vibrationally related to a fully developed carbocation.

The intrinsic 1′-$^{14}$C KIE for the ricin A chain-catalyzed depurination of RNA was 0.993, and this transition state also involves a dissociative oxacarbenium ion (Table 3). The 1′-$^{14}$C KIE for human PNP is 1.002 ± 0.006 within experimental error of that for the ricin A chain. The transition state for human PNP is therefore similar to that of the ricin A chain. The transition state of ricin involves a freely reversible oxacarbenium ion with a chemically significant lifetime. Its formation is followed by an isotopically insensitive, nonchem-

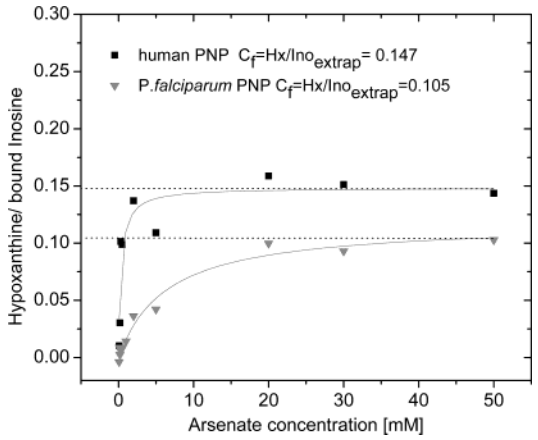


FIGURE 3: Forward commitment experiment for human and *P.f.* PNPs. Mixtures of human or *P.f.* PNP with near-saturating [8-$^{14}$C]inosine were incubated for 10 s and then diluted into excess unlabeled inosine with arsenate at a concentration varied from 0.1 to 50 mM. After 10 s, the reaction was quenched and HPLC analysis used to quantitate hypoxanthine and inosine. The forward commitment factor was calculated at 50 mM arsenate, the concentration used in KIE experiments. The data are fit to the Michaelis−Menten equation, and the lines are the best fits of the data.

ical, and irreversible second step (*25*, *39*). This step provides a transition state with a negligible contribution from reaction coordinate motion. Intrinsic 1′-$^{14}$C KIEs of 0.993 and 1.015 for depurination of RNA and DNA, respectively, by the ricin A chain are sufficiently different to demonstrate that the transition state for DNA depurination also has oxacarbenium ion character but without the requirement of the second step (*40*). The 1′-$^{14}$C KIE for human PNP (1.002) indicates a transition state similar to the equilibrated and fully developed oxacarbenium ion. Bovine PNP has a different transition state, with a 1′-$^{14}$C KIE of 1.022 (*21*). Analysis of the bovine PNP indicates significant bond orders both to the attacking nucleophile (0.03) and to the leaving hypoxanthine (0.32) at the transition state.

*1′-$^{3}$H Kinetic Isotope Effect.* Large α-secondary hydrogen KIEs establish dissociative $A_ND_N$ ($S_N2$ with small bond orders) or $D_N$*$A_N$ ($S_N1$) transition states where $sp^3$ to $sp^2$ rehybridization of C1′ is well developed to give increased freedom to the out-of-plane bending mode and therefore vibrational "looseness" around H1′ (*41*). Small α-secondary hydrogen KIEs indicate symmetric $S_N2$ transition states (*42*). The interpretation of an α-secondary hydrogen KIE into transition state geometry is complicated because this KIE is sensitive to noncovalent and remote interactions (*39*). However, human PNP gives a higher 1′-$^{3}$H KIE (1.184 ± 0.004) than bovine PNP (1.116 ± 0.007), consistent with a more dissociative transition state for human PNP. A similar large α-secondary 1′-$^{3}$H KIE was obtained for RTA-catalyzed RNA depurination (1.163 ± 0.009), also an oxacarbenium ion transition state (*25*). The computed equilibrium isotope effects for 1′-$^{3}$H in formation of a ribooxacarbenium ion in a vacuum are 1.513 and 1.496 for 3′-*exo* and 3′-*endo* conformations, respectively [B1LYP/6-31G(d)]. The maximum experimental α-secondary KIE reported for an $S_N1$ reaction is 1.33 for deuterium (*43*). The α-secondary hydrogen isotope effect is highly sensitive to van der Waals interactions, and these effects certainly occur in the environment of the PNP-stabilized transition state (*44*). Although the 1′-$^{3}$H KIE is consistent with a well-advanced oxacarbenium ion at the transition state, the most unambiguous probe of the transition state is the 1′-$^{14}$C equilibrium isotope effect.

*9-$^{15}$N KIE.* The 9-$^{15}$N KIE of 1.029 ± 0.006 is in good agreement with the theoretical equilibrium isotope effect for hypoxanthine formation of 1.025 computed at the B1LYP/6-31G(d) level of theory. Together with the unity 1′-$^{14}$C KIE (1.002 ± 0.006) for human PNP, these isotope effects establish that the interaction between the ribose moiety and hypoxanthine in the equilibrium oxacarbenium ion is negligible. The 9-$^{15}$N KIE for bovine PNP of 1.010 formed the basis for the relatively large bond order (0.32) between N9 and C1′ at the transition state (*21*). In the case of RTA-catalyzed RNA depurination, the 9-$^{15}$N KIE (1.012) was small despite its highly dissociated transition state (*25*). Small leaving group 9-$^{15}$N isotope effects can arise either from bond preservation in the transition state or by N9 to C1′ bond breaking being compensated by altered conjugation in the purine ring to strengthen the vibrational environment at N9. For human PNP, the large 9-$^{15}$N and small 1′-$^{14}$C isotope effects establish an oxacarbenium ion transition state.

*2′-$^{3}$H Isotope Effect.* Human PNP reveals a small *β*-secondary 2′-$^{3}$H KIE (1.031 ± 0.004) compared to KIEs of 1.12−1.16 reported for other nucleosidases (*17*). The equilibrium isotope effect of 2′-$^{3}$H KIE calculated at the B1LYP/6-31G(d) level of theory for the 3′-*exo* conformation (unconstrained) for ribooxacarbenium ion was 1.214. This conformation gave a p-orbital−C1′−C2′−H2′ dihedral angle of 6.63° where orbital overlap provides strong hyperconjugation between the free p-orbital of the $sp^2$ 1′-C oxacarbenium ion and the C2′−H2′ bond stabilizing the oxacarbenium ion (Figure 5). Systematic analysis [B1LYP/6-31G(d)] of the 2′-$^{3}$H KIE with restraints imposed on the p-orbital−C1′−C2′−H2′ dihedral angle from 0° (full hyperconjugation) to 90° (hyperconjugation disabled) and the O5′−C5′−C4′−C3′ dihedral angle restrained at 46° to match the 5′-$^{3}$H isotope effect (see below) gave a 2′-$^{3}$H EIE from 1.19 for a p-orbital−C1′−C2′−H2′ dihedral angle of 0° in 3′-*exo* to the lower limit of 1.051 for 90° in the 3′-*endo* conformation. The experimental isotope effect of 1.031 is most consistent with the 3′-*endo* conformation. The small *β*-secondary 2′-$^{3}$H isotope effect reveals negligible 2′-hyperconjugation in oxacarbenium ion stabilization, and that condition occurs in only the 3′-*endo* conformation. A 3′-*endo* conformation for the oxacarbenium ion transition state geometry has also been established for the RNA depurination catalyzed by the ricin A chain (*25*). The angular dependence of hyperconjugation has been described for the deuterium KIE and gives a maximal *β*-secondary isotope effect with a dihedral angle of 0° (maximum p-orbital overlap; *45*). After conversion of the tritium to deuterium KIE from the Swain−Schaad relationship (*46*) ($^{T}KIE = {}^{D}KIE^{1.44}$), the 2-$^{3}$H KIE of 1.031 is consistent with the p-orbital−C1′−C2′−H2′ dihedral angle of 57.4° as found in the 3′-*endo* conformation.

*5′-$^{3}$H Kinetic Isotope Effect.* The 5′-$^{3}$H KIE for chemical solvolysis of nucleosides is unity since this bond is not involved in the reaction coordinate. However, the large 5′-$^{3}$H KIE (1.062 ± 0.002) obtained here reveals a large distortion in the vibrational modes of 5′-hydrogens between the free substrate and the transition state. Similar but smaller remote isotope effects have been described for many other

Table 1: Kinetic Isotope Effects for Arsenolysis of Inosine Catalyzed by Human PNP

| substrate | type of KIE | experimental KIE[a] | intrinsic KIE |
|---|---|---|---|
| [1′-$^3$H]- and [5′-$^{14}$C]inosine | α-secondary | 1.160 ± 0.004 | 1.184 ± 0.004 |
| [2′-$^3$H]- and [5′-$^{14}$C]inosine | *β*-secondary | 1.024 ± 0.004 | 1.031 ± 0.004 |
| [1′-$^{14}$C]- and [4′-$^3$H]inosine | primary | 0.981 ± 0.003 | 0.978 ± 0.003 |
| | | 1.002 ± 0.006[b] | 1.002 ± 0.006[b] |
| [9-$^{15}$N/4′-$^3$H]- and [5′-$^{14}$C]inosine | primary | 1.046 ± 0.004 | 1.053 ± 0.004 |
| | | 1.025 ± 0.006[c] | 1.029 ± 0.006[c] |
| [4′-$^3$H]- and [5′-$^{14}$C]inosine | *γ*-secondary | 1.021 ± 0.003 | 1.024 ± 0.003 |
| [5′-$^3$H]- and [5′-$^{14}$C]inosine | *δ*-secondary | 1.054 ± 0.002 | 1.062 ± 0.002 |

[a] Experimental KIEs have been corrected to 0% substrate depletion (eq 4). [b] The 1′-$^{14}$C KIE was corrected for the 4′-$^3$H KIE according to the expression KIE = $KIE_{observed}$ × 4′-$^3$H KIE. [c] The 9-$^{15}$N KIE was corrected for the 4′-$^3$H KIE according to the expression KIE = $KIE_{observed}$/(4′-$^3$H KIE).

Table 2: Kinetic Isotope Effects for Arsenolysis of Inosine Catalyzed by *P.f.* PNP

| substrate | type of KIE | experimental KIE[a] | intrinsic KIE |
|---|---|---|---|
| [1′-$^3$H]- and [5′-$^{14}$C]inosine | α-secondary | 1.105 ± 0.007 | 1.116 ± 0.007 |
| [2′-$^3$H]- and [5′-$^{14}$C]inosine | *β*-secondary | 1.033 ± 0.003 | 1.036 ± 0.003 |
| [1′-$^{14}$C]- and [4′-$^3$H]inosine | primary | 0.988 ± 0.004 | 0.987 ± 0.004 |
| | | 0.996 ± 0.006[b] | 0.996 ± 0.006[b] |
| [9-$^{15}$N/4′-$^3$H]- and [5′-$^{14}$C]inosine | primary | 1.025 ± 0.003 | 1.028 ± 0.003 |
| | | 1.017 ± 0.005[c] | 1.019 ± 0.005[c] |
| [4′-$^3$H]- and [5′-$^{14}$C]inosine | *γ*-secondary | 1.008 ± 0.002 | 1.009 ± 0.002 |
| [5′-$^3$H]- and [5′-$^{14}$C]inosine | *δ*-secondary | 1.058 ± 0.003 | 1.064 ± 0.003 |

[a] Experimental KIEs have been corrected to 0% substrate depletion (eq 4). [b] The 1′-$^{14}$C KIE was corrected for the 4′-$^3$H KIE according to the expression KIE = $KIE_{observed}$ × 4′-$^3$H KIE. [c] The 9-$^{15}$N KIE was corrected for the 4′-$^3$H KIE according to the expression KIE = $KIE_{observed}$/(4′-$^3$H KIE).

Table 3: Comparison of Intrinsic KIEs for Other Purine *N*-Ribosyltransferases

| | | intrinsic KIE | | | |
|---|---|---|---|---|---|
| position | type of KIE | human PNP | *P.f.* PNP | bovine PNP (*21*) | RNA−ricin A chain (*25*) |
| 1′-$^3$H | α-secondary | 1.184 ± 0.004 | 1.116 ± 0.007 | 1.141 ± 0.004 | 1.163 ± 0.009 |
| 2′-$^3$H | *β*-secondary | 1.031 ± 0.004 | 1.036 ± 0.003 | 1.152 ± 0.003 | 1.012 ± 0.004 |
| 1′-$^{14}$C | primary | 1.002 ± 0.006 | 0.996 ± 0.006 | 1.026 ± 0.006 | 0.993 ± 0.004 |
| 9-$^{15}$N | primary | 1.029 ± 0.006 | 1.019 ± 0.005 | 1.010 ± 0.005 | 1.012 ± 0.004 |
| 4′-$^3$H | *γ*-secondary | 1.024 ± 0.003 | 1.009 ± 0.002 | 1.008 ± 0.004 | 0.992 ± 0.004 |
| 5′-$^3$H | *δ*-secondary | 1.062 ± 0.002 | 1.064 ± 0.003 | 1.033 ± 0.005 | 0.996 ± 0.003 |

Table 4: Calculated Equilibrium Isotope Effects for 3-*exo* and 3-*endo* Conformations of Oxacarbenium Ion Formation at the B1LYP/6-31G(d) Level of Theory[a]

| position | 3-*exo* | 3-*endo* | position | 3-*exo* | 3-*endo* |
|---|---|---|---|---|---|
| 1′-$^3$H | 1.5282 | 1.5019 | 4′-$^{18}$O | 0.9831 | 0.9815 |
| 2′-$^3$H | 1.2145 | 1.0584 | 5′-*pro-R*-$^3$H | 0.9983 | 1.0775 |
| 1′-$^{14}$C | 1.0026 | 1.0024 | 5′-*pro-S*-$^3$H | 0.9497 | 0.9883 |
| 9-$^{15}$N | 1.0250 | 1.0250 | total 5′-$^3$H | 0.9481 | 1.0649 |

[a] The equilibrium isotope effects compare inosine and a fully dissociated ribooxacarbenium ion with unconstrained inosine and the ribooxacarbenium ions unconstrained except for the 3-*exo* and 3-*endo* conformations as described in Materials and Methods.

nucleosidases (*17*). The computed 5′-$^3$H equilibrium isotope effect (the product of 5′-*pro-R* and 5′-*pro-S* hydrogen isotope effects) varies between 0.930 for a constrained O5′−C5′−C4′−C3′ dihedral angle of 2° and 1.057 for an angle of 46°. The constrained 3′-*endo* conformation with an O5′−C5′−C4′−C3′ dihedral angle of 46° together with a p-orbital−C1′−C2′−H2′ dihedral angle restrained to 57.3° gives the best fit (1.065) to the experimental value for human PNP of 1.062, while 3′-*exo* conformations give lower values (1.038). The 3′-*endo* conformation of the oxacarbenium ion has the 5′-oxygen positioned over the ribose ring; however, the 5′-hydroxyl hydrogen is free to interact with a hydrogen bond acceptor, known to be histidine in mammalian PNPs (Figure 6). An internal hydrogen bond between O4′ and H5′ can be eliminated, since computational analysis indicated an inverse 5′-$^3$H KIE for this interaction.

A cautionary note for computational analysis of KIE is that the geometry of an oxacarbenium ion in a vacuum will differ from its conformation in PNP. For example, the 5′-$^3$H isotope effect depends on the conformational difference between the free substrate and the transition state. The substrate conformation at the transition state can be estimated from the crystal structures of PNP complexes with transition state analogues bound, but these are only approximate. Despite these limitations, the vibrational frequencies of inosine minimized in vacuo and the computed transition state models provide useful generalization for the transition state structure.

An O5′−C5′−C4′−C3′ dihedral angle of 178° was found for ImmH in the crystal structure with *P. falciparum* PNP. Theoretically, this geometry for the 3′-*exo* conformation of protonated Immucillin-H at the catalytic site of human and *P.f.* PNPs can be transposed to inosine at the transition state. However, there is no proof that inosine conformation is the same as bound ImmH. KIE modeling with restrained 5′-hydroxymethyl group geometry transposed from ImmH to inosine gives a 5′-$^3$H KIE outside the range of the experimental values. Therefore, the unrestrained inosine

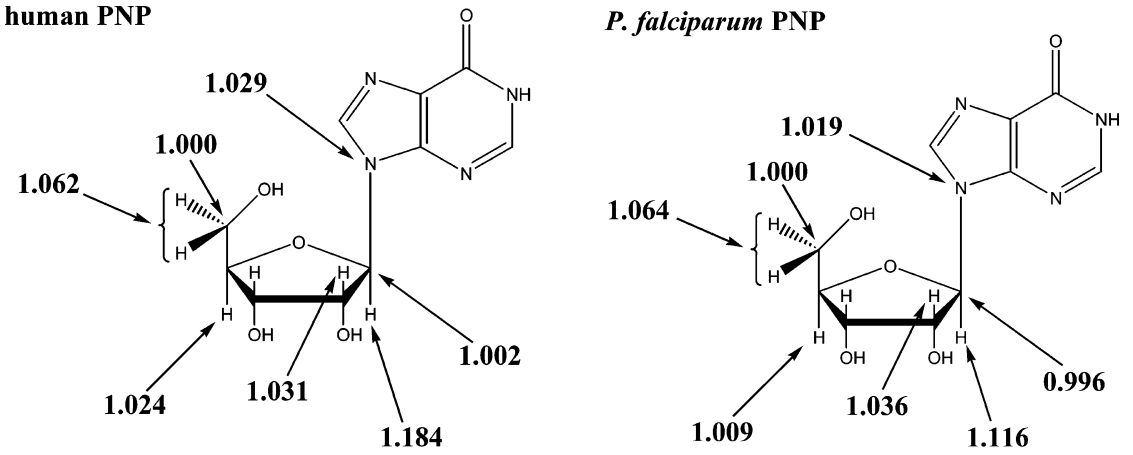


FIGURE 4: Intrinsic kinetic isotope effects for inosine arsenolysis catalyzed by human and *P.f.* PNPs. The KIE from [5′-$^{14}$C]inosine was assumed to be unity and was the control for all other experiments. Error limits on the KIE shown here are reported in Tables 1−3.

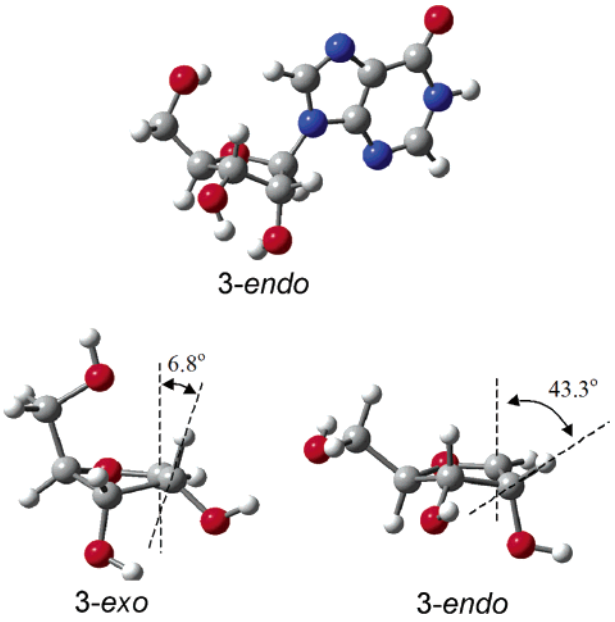


FIGURE 5: Conformations of substrate and oxacarbenium ion optimized at the B1LYP/6-31G(d) level of theory. Minima were found for the 3′-*endo* substrate and 3-*exo* and 3-*endo* oxacarbenium ions. Restraints were imposed in only the initial phase of optimization and removed for final optimization and frequency calculation.

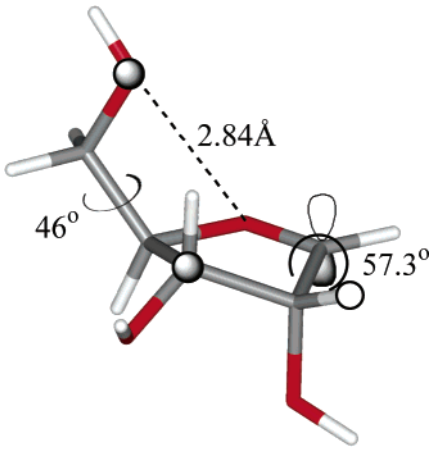


FIGURE 6: Constrained 3′-*endo* oxacarbenium ion conformation. The O5−C5−C4−C3 dihedral angle was constrained to 46° to match the experimental 5′-tritium isotope effects. The p-orbital−C1−C2−H2 dihedral angle of 57.3° (shown for human PNP) or 55.7° (for *P.f.* PNP) corresponding to the 3-*endo* conformation was found from the angular dependence of the 2′-$^{3}$H KIE (see the text for details).

geometry (O5′−C5′−C4′−C3′ dihedral angle of 63°) was used for KIE calculations.

From the 5′-$^{3}$H KIE, it is clear that the transition state holds the 5′-hydroxymethyl in a geometry that weakens C−H 5′-bonds relative to those in the free substrate. This feature of the transition state is not important for the design of transition state analogues since conformational freedom of rotation of the 5′-group permits conformational adjustment for the 5′-group geometry.

*P. falciparum PNP Isotope Effects. 1′-$^{14}$C Isotope Effects.* A slightly inverse 1′-$^{14}$C KIE (0.996) identifies the *P. falciparum* transition state as being similar to the oxacarbenium ion of RTA for RNA depurination. A transition state closely related to the oxacarbenium ion intermediate (described above) for human PNP is implicated, with no significant contribution from 1′-C reaction coordinate motion.

*9-$^{15}$N Kinetic Isotope Effect.* The value of 1.019 for the 9-$^{15}$N KIE is smaller than the equilibrium isotope effect of 1.025 computed for a fully dissociated transition state [modeled at the B1LYP/6-31G(d) level of theory]. A reduced 9-$^{15}$N KIE indicates a more constrained vibrational environment for N9 at the transition state of *P. falciparum* PNP. Loss of the C1′−N7 bond must therefore be compensated by altered conjugation in the leaving group.

*N7 Protonation State.* Proton transfer to the 7-nitrogen proposed in previous transition state analyses of purine nucleosidases is consistent with the 9-$^{15}$N isotope effect obtained here. The hypoxanthine anion would be a poor leaving group, and protonation at N7 forms the neutral purine. Protonation at N7 also increases the N9−C8 bond order in the N7-protonated hypoxanthine tautomer, partially conserving the net bond order around N9.

*Solvent $D_2O$ Isotope Effects.* The $V_{max}/K_m$ solvent deuterium isotope effects for arsenolysis catalyzed by *P.f.* are 1.6 and 1.3 in 2.5 and 50 mM arsenate, respectively. These small solvent effects are consistent with protonation of N7 being nearly complete prior to forming the transition state. Solvent deuterium isotope effects of 3−6 would be expected if the proton is in motion at the transition state (*38*). Solvent deuterium isotope effects for human PNP are larger at 2.5 and 1.8 in 2.5 and 50 mM arsenate, respectively. The solvent isotope effects correlate with the 9-$^{15}$N equilibrium isotope

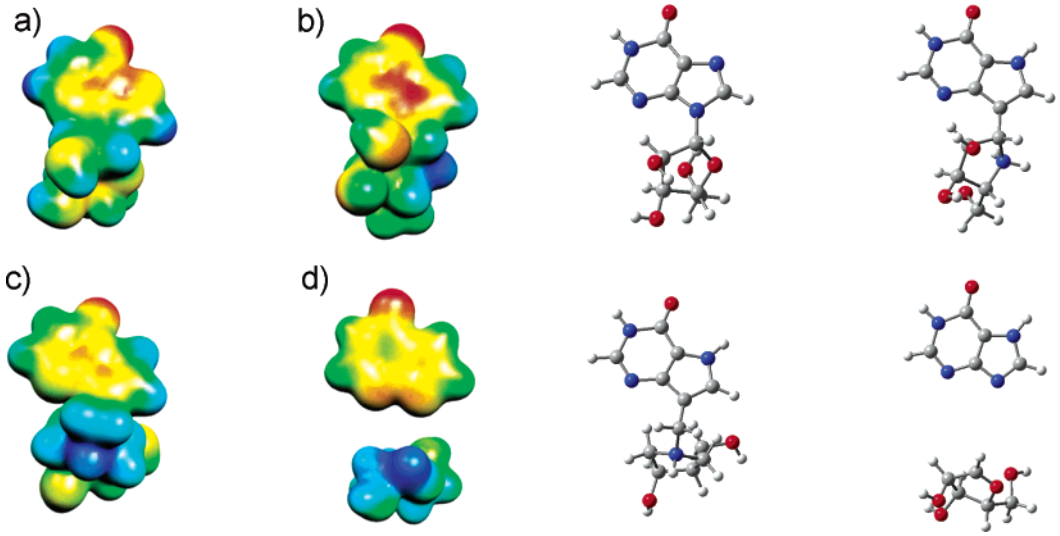


FIGURE 7: Molecular electrostatic potential surfaces (MEPs) for inosine (a), Immucillin-H (b), DADMe-Immucillin-H (c), and the oxacarbenium/hypoxanthine pair (d). MEP were calculated at the HF/STO-3G level of theory (*Gaussian 98*/cube) for the optimized geometry at the B1LYP/6-31G(d) level of theory and visualized with Molekel 4.0 at a density of 0.008 electron/bohr. The ball-and-stick models shown at the right have the same geometry as the MEP surfaces.

effects for both human and *P.f.* PNPs since the net bond order at N9 is increased by full protonation at N7.

*2′-$^3$H KIE*. The $\beta$-secondary 2′-$^3$H KIE of 1.036 for *P.f.* PNP is not significantly different from that of human PNP (1.031) and also corresponds to that of the 3′-*endo* conformation with a p-orbital−C1′−C2′−H2′ dihedral angle of 55.7°. The difference of 1.7° is not significant.

*5′-$^3$H Kinetic Isotope Effect*. The 5′-$^3$H isotope effects of 1.064 and 1.062 for *P.f.* and human PNPs, respectively, establish the same conformations of the 5′-hydroxymethyl at these transition states. The presence of His7/His257 in H-bonds to both 5′-hydroxyls suggests similar anchoring of the 5′-hydroxyl groups.[2]

*1′-$^3$H Kinetic Isotope Effect*. The most striking difference between human and *P.f.* PNP isotope effects concerns the α-secondary 1′-$^3$H kinetic isotope effects. The value of 1.116 ± 0.007 for *P.f.* PNP is almost 7% lower than the human 1′-$^3$H KIE (1.184 ± 0.004). Clearly, the vibrational environment at the transition state of *P.f.* PNP is stiffer than for the human PNP. The peptide carbonyl oxygens of Ser91 in *P.f.* PNP or Ala116 in human PNP are near the 1′-carbon position of transition state analogue inhibitors crystallized in the catalytic sites.[2] Distances of 4.02 Å for human PNP and 3.33 Å for *P.f.* PNP suggest that these van der Waals contacts may suppress the α-tritium isotope effect for carbocation formation at the transition state. The unpolarized 1′-hydrogen of inosine is a poor candidate for hydrogen bond formation; however, the strongly polarized 1′-carbon−hydrogen bond in the oxacarbenium ion has the potential to interact with these peptide carbonyl groups. Interactions between PNPs and H1′ at the transition states have the potential to decrease the 1′-$^3$H KIE for *P.f.* PNP; however, computational modeling with a single carbonyl oxygen fixed at 3.3 Å was unable to show such charges. This distance occurs with analogues of the transition state, and the actual transition state may well be characterized by closer interactions.

The 1′-$^3$H and 9-$^{15}$N kinetic isotope effects of *P.f.* PNP are smaller than for human PNP. Therefore, the oxacarbenium ion transition state for *P.f.* is more constrained in its vibrational modes. Apart from the speculation provided above, the physical and chemical bases for these differences are unknown.

*Molecular Electrostatic Potential Surface Analysis*. The proposed $D_N$*$A_N$ mechanisms passing through stabilized oxacarbenium ions are consistent with the binding affinities of transition state analogue inhibitors. The methylene bridge in DADMe-ImmH makes the 9-deazahypoxanthine leaving group analogue more distant from the oxacarbenium ion mimic than in ImmH (*24*; Figures 1 and 7). The dissociation constant is improved from 56 pM for ImmH to 16 pM for DADMe-ImmH against human PNP (*24*, *47*). However, no change is observed for *P.f.* PNP, giving a $K_i$ of 0.6 nM for ImmH and a $K_i$ of 0.5 nM for DADMe-ImmH.[3]

Increased separation between the oxacarbenium mimic and 9-deazahypoxanthine is not the sole cause of binding improvement. Although 1′,9-methylene-ImmH also has increased separation between the oxacarbenium mimic and 9-deazahypoxanthine, its binding to human PNP is weak ($K_i$ = 250 nM; *23*).[3] The positive charge at N1′ of DADMe-ImmH mimics the charge distribution of the oxacarbenium intermediate, localized primarily at C1′ with a slight hyperconjugation between the C1′ p-orbital and the C2′−H2′ bond, revealed by the small 2′-$^3$H isotope effect. Molecular electrostatic potential analysis shows a similar charge distribution for oxacarbenium/hypoxanthine and DADMe-ImmH (Figure 7).

*Transition State Ion Pair Hypothesis and KIEs*. The observation that an ion pair forms at the catalytic sites of PNPs between $PO_4$ and N1′ of DADMe-Immucillin-H and is responsible for tight binding (*23*) suggests that a similar ion pair may form at the transition state between $PO_4$ and the ribooxacarbenium ion. To be consistent with the contri-

[2] Unpublished results of the X-ray crystal structures of human and *P.f.* PNPs.

[3] Unpublished results of the inhibitor specificity of human and *P.f.* PNPs.

bution of negligible reaction coordinate motion to the kinetic isotope effect, the stabilized ribooxacarbenium ion requires a stationary position between the hypoxanthine leaving group and the phosphate anion. If the 1′-carbon and phosphate oxygen interaction causes motion at the transition state, the 1′-$^{14}$C KIE should be greater than unity. However, it is possible that the equilibrium isotope effect on oxacarbenium ion formation is slightly inverse and the [1′-$^{14}$C]carbocation−phosphate interaction provides a small normal KIE from reaction coordinate contribution so the combined effect is near unity. An inverse EIE of 0.983 for carbocation formation has been observed for the equilibrium between triphenylmethyl chloride and triphenylmethyl cation (*48*). This possibility cannot be experimentally resolved from the data presented here, but is a possibility that could include a small contribution of not more than 1.5% of the 1′-$^{14}$C KIE from reaction coordinate motion.

## CONCLUSIONS

Kinetic isotope effect analysis for human and *P.f.* PNPs has implicated a mechanism where relatively stable oxacarbenium ions are formed. The mechanism is different from that previously characterized for bovine PNP. The transition states for human and *P.f.* PNP resemble those for ricin A chain depurination of RNA. The oxacarbenium ion formed by *P.f.* PNP is possibly followed by an irreversible and isotopically insensitive step. The vibrational environment for the oxacarbenium ion in the active site of *P.f.* PNP is more constraining than for human PNP, especially around the hypoxanthine leaving group. Differences in the hydrogen bonds to the leaving group or different van der Waals interaction with the ribooxacarbenium ion could account for these constraints.

The small differences between human and *P. falciparum* PNP kinetic isotope effects support similar transition state structures, yet steps leading to these transition states are different. *P.f.* PNP has a lower $K_m$ for inosine (5 $\mu$M vs 38 $\mu$M for human PNP), and the $k_{cat}$ for *P.f.* PNP is slower than the value for human PNP by a factor of 100 (*6*). On the basis of the similarity of the transition states, but the lower intrinsic rate acceleration provided by *P.f.* PNP, the malarial enzyme differs from human PNP in the weaker binding of the transition state ensemble or differences in the rate of the isotopically insensitive step(s) following transition state formation.

## ACKNOWLEDGMENT

We gratefully acknowledge Dr. Wuxian Shi from the Albert Einstein College of Medicine (AECOM) Department of Biochemistry, Dr. Li-Min Ting from the AECOM Departament of Microbiology and Immunology for the generous gift of *P. falciparum* PNP, Dr. Charles Grubmeyer (Temple University) for adenosine phosphoribosyltransferase (APRTase), and Dr. Paul Berti (McMaster University) for 5′-phosphoribosylpyrophosphate synthetase (PRPPase).

## REFERENCES

1. Krudsood, S., Buchachart, K., Chalermrut, K., Charusabha, C., Treeprasertsuk, S., Haoharn, O., Duangdee, C., and Looareesuwan, S. (2002) A comparative clinical trial of combinations of dihydroartemisinin plus azithromycin and dihydroartemisinin plus mefloquine for treatment of multidrug resistant falciparum malaria, *Southeast Asian J. Trop. Med. Public Health 33*, 525−531.
2. Winstanley, P. A., Ward, S. A., and Snow, R. W. (2002) Clinical status and implications of antimalarial drug resistance, *Microbes Infect. 4*, 157−164.
3. Sherman, I. W. (1979) Biochemistry of *Plasmodium* (malarial parasites), *Microbiol. Rev. 43*, 453−495.
4. Subbayya, I. N., Ray, S. S., Balaram, P., and Balaram, H. (1997) Metabolic enzymes as potential drug targets in *Plasmodium falciparum*, *Indian J. Med. Res. 106*, 79−94.
5. Queen, S. A., Jagt, D. L., and Reyes, P. (1990) In vitro susceptibilities of *Plasmodium falciparum* to compounds which inhibit nucleotide metabolism, *Antimicrob. Agents Chemother*. *34*, 1393−1398.
6. Kicska, G. A., Tyler, P. C., Evans, G. B., Furneaux, R. H., Kim, K., and Schramm, V. L. (2002) Transition state analogue inhibitors of purine nucleoside phosphorylase from *Plasmodium falciparum*, *J. Biol. Chem*. *277*, 3219−3225.
7. Kicska, G. A., Tyler, P. C., Evans, G. B., Furneaux, R. H., Schramm, V. L., and Kim, K. (2003) Purine-less death in *Plasmodium falciparum* induced by Immucillin-H, a transition state analogue of purine nucleoside phosphorylase, *J. Biol. Chem. 277*, 3226−3231.
8. Kicska, G. A., Long, L., Horig, H., Fairchild, C., Tyler, P. C., Furneaux, R. H., Schramm, V. L., and Kaufman, H. L. (2001) Immucillin H, a powerful transition-state analog inhibitor of purine nucleoside phosphorylase, selectively inhibits human T lymphocytes, *Proc. Natl. Acad. Sci. U.S.A. 98*, 4593−4598.
9. Banti, S., Miller, P. J., Parker, C. D., Ananth, S. L., Horn, L. L., Babu, Y. S., and Sandhu, J. S. (2002) Comparison of in vivo efficacy of BCX-1777 and cyclosporin in xenogeneic graft-vs.-host disease: the role of dGTP in antiproliferative action of BCX-1777, *Int. Immunopharmacol. 2*, 913−923.
10. Pugmire, M. J., and Ealick, S. E. (2002) Structural analyses reveal two distinct families of nucleoside phosphorylases, *Biochem. J. 361*, 1−25.
11. Schramm, V. L. (2002) Development of transition state analogues of purine nucleoside phosphorylase as anti-T-cell agents, *Biochim. Biophys. Acta 1587*, 107−117.
12. Datta, N. S., Shewach, D. S., Mitchell, B. S., and Fox, I. H. (1989) Kinetic properties and inhibition of human T lymphoblast deoxycytidine kinase, *J. Biol. Chem*. *264*, 9359−9364.
13. Bzowska, A., Kulikowska, E., and Shugar, D. (2000) Purine nucleoside phosphorylase: properties, functions, and clinical aspects, *Pharmacol. Ther*. *88*, 349−425.
14. Giblett, E. R., Ammann, A. J., Wara, D. W., Sandman, R., and Diamond, L. K. (1975) Nucleoside phosphorylase deficiency in a child with severely defective T-cell immunity and normal B-cell immunity, *Lancet 1*, 1010−1013.
15. Bantia, S., Ananth, S. L., Parker, C. D., Horn, L. L., and Upshaw, R. (2003) Mechanism of inhibition of T-acute lymphoblastic leukemia cells by PNP inhibitor BCX-1777, *Int. Immunopharmacol*. *3*, 879−887.
16. Schramm, V. L. (2003) Enzymatic transition state poise and transition state analogues, *Acc. Chem. Res. 36*, 588−596.
17. Schramm, V. L. (1999) Enzymatic transition-state analysis and transition-state analogs, *Methods Enzymol. 308*, 301−355.
18. Schramm, V. L., Horenstein, B. A., and Kline, P. C. (1994) Transition state analysis and inhibitor design for enzymatic reactions, *J. Biol. Chem*. *269*, 18259−18262.
19. Schramm, V. L. (2001) Transition state variation in enzymatic reactions, *Curr. Opin. Chem. Biol. 5*, 556−563.
20. Cook, P. F. (1991) *Enzyme Mechanism from Isotope Effects*, p 4, CRC Press, Boca Raton, FL.
21. Kline, P. C., and Schramm, V. L. (1993) Purine nucleoside phosphorylase. Catalytic mechanism and transition-state analysis of the arsenolysis reaction, *Biochemistry 32*, 13212−13219.
22. Kicska, G. A., Tyler, P. C., Evans, G. B., Furneaux, R. H., Shi, W., Fedorov, A., Lewandowicz, A., Cahill, S. M., Almo, S. C., and Schramm, V. L. (2002) Atomic dissection of the hydrogen bond network for transition-state analogue binding to purine nucleoside phosphorylase, *Biochemistry 41*, 14489−14498.
23. Lewandowicz, A., Shi, W., Evans, G. B., Tyler, P. T., Furneaux, R. H., Basso, L. A., Santos, D. S., Almo, S. C., and Schramm, V. L. (2003) Over-the-barrier transition state analogues and crystal structure with *Mycobacterium tuberculosis* purine nucleoside phosphorylase, *Biochemistry 42*, 6057−6066.
24. Lewandowicz, A., Tyler, P. C., Evans, G. B., Furneaux, R. H., and Schramm, V. L. (2003) Achieving the ultimate goal in

transition state analogues for human purine nucleoside phosphorylase, *J. Biol. Chem. 34*, 31465−31468.
25. Chen, X.-Y., Berti, P. J., and Schramm, V. L. (2000) Ricin A-chain: Kinetic isotope effects and transition state structure with stem-loop RNA, *J. Am. Chem. Soc. 122*, 1609−1617.
26. McIvor, R. S., Goddar, J. M., Simones, C. C., and Martin, D. W., Jr. (1985) Expression of cDNA sequence encoding human purine nucleoside phosphorylase in rodent and human cells, *Mol. Cell. Biol. 5*, 1349−1357.
27. Rising, K. A., and Schramm, V. L. (1994) Enzymatic Synthesis of $NAD^+$ with the Specific Incorporation of Atomic Labels, *J. Am. Chem. Soc. 116*, 6531−6536.
28. Parkin, D. W., Leung, H. B., and Schramm, V. L. (1984) Synthesis of nucleotides with specific radiolabels in ribose. Primary $^{14}C$ and secondary $^3H$ kinetic isotope effects on acid-catalyzed glycosidic bond hydrolysis of AMP, dAMP, and inosine, *J. Biol. Chem. 259*, 9411−9417.
29. Miles, R. W., Tyler, P. C., Furneaux, R. H., Bagdassarian, C. K., and Schramm, V. L. (1998) One-third-the-sites transition-state inhibitors for purine nucleoside phosphorylase, *Biochemistry 37*, 8615−8621.
30. Rose, I. A. (1980) The isotope trapping method: desorption rates of productive E.S complexes, *Methods Enzymol. 64*, 47−59.
31. Frisch, M. J., Trucks, G. W., Schlegel, H. B., Scuseria, G. E., Robb, M. A., Cheeseman, J. R., Zakrzewski, V. G., Montgomery, J. A., Jr., Stratmann, R. E., Burant, J. C., Dapprich, S., Millam, J. M., Daniels, A. D., Kudin, K. N., Strain, M. C., Farkas, O. J., Tomasi, B. V., Cossi, M., Cammi, R., Mennucci, B., Pomelli, C., Adamo, C., Clifford, S., Ochterski, J., Petersson, G. A., Ayala, P. Y., Cui, Q., Morokuma, K., Malick, D. K., Rabuck, A. D., Raghavachari, K., Foresman, J. B., Cioslowski, J., Ortiz, J. V., Stefanov, B. B., Liu, G., Liashenko, A., Piskorz, P., Komaromi, I., Gomperts, R., Martin, R. L., Fox, D. J., Keith, T., Al-Laham, M. A., Peng, C. Y., Nanayakkara, A., Gonzalez, C., Challacombe, M., Gill, P. M. W., Johnson, B., Chen, W., Wong, M. W., Andres, J. L., Gonzalez, C., Head-Gordon, M., Replogle, E. S., and Pople, J. A. (1998) *Gaussian 98*, revision A.9, Gaussian, Pittsburgh, PA.
32. Becke, D. A. (1996) Density-functional thermochemistry. IV. A new dynamical correlation functional and implications for exact-exchange mixing, *J. Chem. Phys. 104*, 1040−1046.
33. Anisimov, V., and Paneth, P. (1999) ISOEFF98. A program for studies of isotope effects using Hessian modifications, *J. Math. Chem. 26*, 75−86.
34. Melander, L., and Saunders, W. H., Jr. (1980) *Reaction Rates of Isotopic Molecules*, Wiley and Sons, New York.
35. Flükiger, P., Lüthi, H. P., Portmann, S., and Weber, J. (2000) *MOLEKEL 4.0*, Swiss Center for Scientific Computing, Manno, Switzerland.
36. Bagdassarian, C. K., Shramm, V. L., and Schwartz, S. D. (1996) Molecular electrostatic potential analysis for substrates, competitive inhibitors and transition state inhibitors, *Biochemistry 37*, 8825−8836.
37. Parkin, D. W. (1991) in *Enzyme Mechanism from Isotope Effects* (Cook, P. F., Ed.) pp 269−290, CRC Press, Boca Raton, FL.
38. Horenstein, B. A., Parkin, D. W., Estupinan, B., and Schramm, V. L. (1991) Transition-state analysis of nucleoside hydrolase from *Crithidia fasciculata*, *Biochemistry 30*, 10788−10795.
39. Berti, P. J., and Tanaka, K. S. E. (2002) Transition state analysis using multiple kinetic isotope effects: mechanism of enzymatic and non-enzymatic glycoside hydrolysis and transfer, *Adv. Phys. Org. Chem. 37*, 239−314.
40. Chen, X.-Y., Berti, P. J., and Schramm, V. L. (2000) Transition state analysis for depurination of DNA by ricin A-chain, *J. Am. Chem. Soc. 122*, 6527−6534.
41. Pham, T. V., Fang, Y.-R., and Westaway, K. C. (1997) Using secondary deuterium kinetic isotope effects to determine the symmetry of $S_N2$ transition states, *J. Am. Chem. Soc. 119*, 3670−3676.
42. Glad, S. S., and Jensen, F. (1997) Transition state looseness and $\beta$-secondary kinetic isotope effects, *J. Am. Chem. Soc. 119*, 227−232.
43. Adcock, W., Trout, N. A., Vercoe, D., Taylor, D. K., Shiner, V. J., Jr., and Sorensen, T. S. (2003) Solvolysis of (*Z*)-5-trimethylstannyl 2-adamantyl *p*-bromobenzenesulfonate: mechanistic implications of a record-breaking secondary-deuterium kinetic isotope effect for an $S_N1$ substrate, *J. Org. Chem. 68*, 5399−5402.
44. Poirier, R. A., Wang, Y., and Westaway, K. C. (1994) A theoretical study of the relationship between secondary alpha-deuterium kinetic isotope effects and the structure of $S_N2$ transition states, *J. Am. Chem. Soc. 116*, 2526−2533.
45. Sunko, D. E., Szele, I., and Hehre, W. J. (1977) Hyperconjugation and the angular dependence of beta-deuterium isotope effects, *J. Am. Chem. Soc. 99*, 5000−5005.
46. Swain, C. G., Stivers, E. C., Reuver, J. F., Jr., and Schaad, L. J. (1958) Use of hydrogen isotope effect to identify the attacking nucleophile in the enolization of ketones catalyzed by acetic acid, *J. Am. Chem. Soc. 80*, 5885−5893.
47. Evans, G. B., Furneaux, R. H., Lewandowicz, A., Schramm, V. L., and Tyler, P. C. (2003) Exploring structure−activity relationships of transition state analogues of human purine nucleoside phosphorylase, *J. Med. Chem. 46*, 3412−3423.
48. Kresge, A. J., Lichtin, N. N., Rao, K. N., and Weston, R. E. (1965) The primary carbon isotope effect on the ionization of triphenylmethyl chloride. Experimental determination, theoretical justification, and implications for carbon isotope effects on nucleophilic substitution at saturated carbon, *J. Am. Chem. Soc. 87*, 437−445.

BI0359123